



# New model to predict thermomagnetic properties of nanostructured magnetic compounds

Denis Gokhfeld<sup>1</sup> · Michael Rudolf Koblischka<sup>2</sup> · Anjela Koblischka-Veneva<sup>2</sup>

Received: 21 September 2024 / Accepted: 23 November 2024 / Published online: 12 December 2024  
© The Author(s) 2024

## Abstract

The development of new materials showing the magneto-caloric effect (MCE) requires fast and reliable characterization methods. For this purpose, a phenomenological model developed by M. A. Hamad has proven to be a useful tool to predict the magnetocaloric properties (the isothermal magnetic entropy change,  $\Delta S_M$ , the magnetization-related change of the specific heat,  $\Delta C_{P,H}$ , and the relative cooling power, RCP) via calculation from magnetization measurements as a function of temperature,  $M(T)$ . However, fitting the  $M(T)$  data is difficult for broad, smoothed-out transition curves which are often observed for material systems such as core-shell nanoparticles, nanowires, nanowire fabrics or nanoparticle hybrid materials. Thus, in this contribution we present a different approach enabling proper fitting of such magnetization data via the use of an asymmetric Boltzmann sigmoid function, which provides a clear physical background and enables to properly describe the broad and smoothed out transitions of nanomaterials. As examples for our procedure, we present fits to  $M(T)$  curves of polycrystalline, bulk  $\text{La}_{0.67}\text{Ba}_{0.33}\text{MnO}_3$  as well as  $\text{La}_{1-x}\text{Sr}_x\text{MnO}_3$  ( $x = 0.2, 0.3, 0.4$ ) and  $\text{La}_{0.7}\text{Ca}_{0.3}\text{MnO}_3$  nanostructured materials from various authors.

**Keywords** MCE effect · Curie temperature · Paramagnetic–ferromagnetic transition · Modelling

## 1 Introduction

The growing importance of green technology for the modern world caused increased interest in technologies like magnetic refrigeration, based on the magneto-caloric effect (MCE) [1]. In principle, any magnetic material may exhibit this effect, with mostly weak effects at elevated temperatures. However, at temperatures in the vicinity of room temperature (RT) or above, only some types of materials were found with a reasonably large MCE effect; the most prominent one being metallic Gd. Such materials were reviewed

in Refs. [2–7]. Among them, the ceramic materials of the perovskite-type manganites (generic formula  $A_{1-x}B_x\text{MnO}_3$ ) offer high Curie temperatures ( $T_C$ ) well above RT [8–10], leading to considerable research efforts to find new materials with even higher  $T_C$ 's, e.g., by chemical doping [11–14]. Thus, it is essential for the ongoing material research to have an easily applicable set of tools to measure the MCE properties of a given material.

A common approach to achieve this goal is the magnetic measurement of the ferromagnetic transition curve ( $M(T)$ ) in the vicinity of the Curie temperature as outlined by Földeaki et al. [15]. From the measured  $M(T)$  data, the isothermal magnetic entropy change  $\Delta S_M$ , can be calculated, enabling further the determination of several other parameters such as the magnetization-related change of the specific heat,  $\Delta C_{P,H}$ , the relative cooling power (RCP) [16], etc. However, the required calculation process remains somewhat tedious, and so a phenomenological model was developed in order to provide a more straightforward data handling. In 2012, Hamad suggested a phenomenological expression to fit the magnetization data ( $M(T)$ ) recorded during the ferromagnetic–paramagnetic transition in Refs. [17–19]:

✉ Michael Rudolf Koblischka  
m.koblischka@gmail.com

Denis Gokhfeld  
gokhfeld@iph.krasn.ru

Anjela Koblischka-Veneva  
a.koblischka@gmail.com

<sup>1</sup> Kirensky Institute of Physics, Krasnoyarsk Scientific Center, Siberian Branch, Russian Academy of Sciences, 660036 Krasnoyarsk, Russia

<sup>2</sup> Experimental Physics, Saarland University, P.O. Box 151150, 66041 Saarbrücken, Germany

$$M(T) = \frac{M_i - M_f}{2} \tanh [-A(T - T_C)] + BT + C, \tag{1}$$

where  $M_i$  and  $M_f$  are the initial and final values of the magnetization in a ferromagnetic–paramagnetic transition. The values of the parameters  $A$  and  $C$  are defined as  $A = 2(B - S_c)/(M_i - M_f)$ ,  $C = (M_i + M_f)/2 - BT_C$ , where  $B$  denotes the magnetization sensitivity  $dM/dT$  below  $T_C$ , and  $S_c$  represents the magnetization sensitivity,  $dM/dT$ , at  $T_C$ . The Hamad’s formula as given in Eq. (1) appeared to be a convenient tool for estimating the parameters of the MCE such as  $\Delta S_M$ , RCP, and  $\Delta C_{P,H}$  and was employed by Hamad’s group and as well by other authors in the literature. This model proved to be especially useful to treat noisy magnetization curves or  $M(T)$  data recorded with only a small number of data points, which are difficult to be processed further. An analytical expression can be used to fit such  $M(T)$  curves and to obtain  $\Delta S_M$  and  $\Delta C_{P,H}$ . Usually, the most often considered magnetic materials exhibit a steep transition between the ferromagnetic and paramagnetic states, and so the Hamad approach works well. However, recently developed material systems such as core-shell nanoparticles, nanowires, nanowire fabrics or nanoparticle hybrid materials [5, 20–23] show up with broad, smoothed-out transition curves and are, therefore, only poorly fit by Hamad’s formula.

The change in the system parameters during a phase transition can be described by the Boltzmann sigmoid function, as done by many authors in many different fields like growth processes, polymer transitions, smart gels as well as superconductivity [24–29]. To our knowledge, this function was not yet applied to ferromagnetic–paramagnetic transitions. Thus, in the current contribution, we present a different approach based on the Boltzmann sigmoid function to enable a proper fitting of magnetization data of nanostructured magnetic materials.

## 2 Model

The Boltzmann sigmoid function arises as a result of minimizing the change in free energy due to a phase transition [24]. Using the Boltzmann sigmoid function, the magnetization during ferromagnetic–paramagnetic transition can be expressed as

$$M(T) = M_i(T) + \frac{M_f(T) - M_i(T)}{1 + \exp(-(T - T_C)/T_w)}, \tag{2}$$

where  $T_w$  is a parameter characterizing the transition width. This expression has clear physical sense and describes a transition from the state with magnetization  $M_i(T)$  to the state with magnetization  $M_f(T)$ . Given  $T_w = 1/(2A)$ ,  $M_i(T) = M_i + B(T - T_C)$ , and  $M_f(T) = M_f - B(T - T_C)$ , the expression (2) can be transformed to the Hamad’s formula

(1). Therefore, the Hamad’s phenomenological formula (1) and the approach suggested here using the Boltzmann sigmoid function (2) are analogous.

In a broad and smoothed transition between the ferromagnetic and paramagnetic states often seen for nanostructured materials, the magnetization is changed in a different manner at  $T$  below  $T_C$  and at  $T$  above  $T_C$ . To be able fit this behavior properly, we choose an asymmetric sigmoid function [30]. Then, the ferromagnetic–paramagnetic transition in nanostructured materials is described by the following expression:

$$M(T) = M_i(T) + \frac{M_f(T) - M_i(T)}{[1 + \nu \exp(-(T - T_C)/T_w)]^{1/\nu}}, \tag{3}$$

where  $\nu$  is a dimensionless parameter accounting for the asymmetry, which depends on a characteristic size and/or structural disorder.  $M_i(T)$  and  $M_f(T)$  can be expressed as  $M_i(T) = M_i + S_i(T - T_C)$  and  $M_f(T) = M_f + S_f(T - T_C)$ , where  $S_i$  and  $S_f$  are the magnetization sensitivities  $dM/dT$  above and below  $T_C$ , respectively. Like the function (2), function (3) has a derivative extremum at  $T = T_C$ .

Values of the magnetic entropy change  $\Delta S_M$ , the relative cooling power RCP, and the magnetization-related change of the specific heat  $\Delta C_{P,H}$  can now be obtained by numerical calculations from Eq. (3), using

$$\begin{aligned} \Delta S_M(T, H) &= \mu_0 \int_0^H \frac{\partial M(T, H')}{\partial T} dH', \\ \text{RCP}(T, H) &= -\Delta S_M(T, H) \delta T_{\text{FWHM}}, \\ \Delta C_{P,H}(T) &= T \frac{\delta \Delta S_M(T, H)}{\delta T}, \end{aligned} \tag{4}$$

where  $\delta T_{\text{FWHM}}$  is a full-width at half-maximum of a  $\Delta S_M(T, H)$  dependence. Let us set  $M_i(T) = M_i$  and  $M_f(T) = M_f$ , which is valid in the vicinity of a ferromagnetic–paramagnetic transition, to find analytical expressions for thermomagnetic parameters from Eq. (3). The magnetic entropy change  $\Delta S_M$  is derived from Eq. (3):

$$\Delta S_M(T, H) = -\frac{\mu_0 H}{T_w} \frac{(M_i - M_f) \exp\left(-\frac{T - T_C}{T_w}\right)}{\left[1 + \nu \exp\left(-\frac{T - T_C}{T_w}\right)\right]^{\frac{1}{\nu} + 1}}. \tag{5}$$

Here, the values of  $\Delta S_M$  are given in J/(kg K) and the values of magnetization are expressed in A m<sup>2</sup>/kg. The maximum change  $\Delta S_{\text{Max}}$  is calculated as

$$\Delta S_{\text{Max}}(T, H) = -\frac{\mu_0 H}{T_w} \frac{(M_i - M_f)}{(\nu + 1)^{\frac{1}{\nu} + 1}}. \tag{6}$$

To obtain  $\delta T_{\text{FWHM}}$ , the full-width at half-maximum of a  $\Delta S_M(T, H)$  dependence, one should find two roots  $T_1$  and  $T_2$

of the equation  $\Delta S_M - 0.5\Delta S_{Max} = 0$ . For  $\nu = 1$ ,  $\delta T_{FWHM}$  is given by

$$\delta T_{FWHM} = \left[ \ln(3 + \sqrt{8}) - \ln(3 - \sqrt{8}) \right] T_w \approx 3.53T_w.$$

For  $\nu > 1$ , the values of  $\delta T_{FWHM}$  are calculated numerically. The  $\delta T_{FWHM}$  values for different  $\nu$  can be approximated by

$$\delta T_{FWHM} \approx (0.78\nu + 2.75)T_w, \tag{7}$$

The relative cooling power based on the magnetic entropy change is obtained via

$$RCP \approx \mu_0 H (M_i - M_f) \frac{0.78\nu + 2.75}{(\nu + 1)^{\frac{1}{\nu} + 1}}. \tag{8}$$

The magnetization-related change of the specific heat,  $\Delta C_{P,H}$  is expressed as

$$\Delta C_{P,H}(T) = \mu_0 H \frac{T}{T_w^2} \frac{(M_i - M_f) \exp\left(-\frac{T-T_c}{T_w}\right) \left[1 - \exp\left(-\frac{T-T_c}{T_w}\right)\right]}{\left[1 + \nu \exp\left(-\frac{T-T_c}{T_w}\right)\right]^{\frac{1}{\nu} + 2}}. \tag{9}$$

Using this set of improved formulae, a better fitting of experimentally measured  $M(T)$ -data found in the literature can be achieved. This is shown in the following Section for some examples. Here, we have chosen data of perovskite-type manganites as for these materials, data of bulk samples and nanostructured ones are available in the literature.

### 3 Application of the model and discussion

One of the first papers of Hamad [18] was using the data of  $\text{La}_{0.67}\text{Sr}_{0.33}\text{MnO}_3$  (LSMO) and  $\text{La}_{0.67}\text{Ca}_{0.33}\text{MnO}_3$  (LCMO) polycrystalline bulk samples measured at  $H = 500$  Oe presented in Refs. [8, 31, 32] for the introduction of his phenomenological model. However, in Refs. [8, 31, 32] data were included for two applied magnetic fields of 500 Oe and 20 kOe and also data for a  $\text{La}_{0.67}\text{Ba}_{0.33}\text{MnO}_3$  (LBMO) polycrystalline, bulk sample were shown. LBMO exhibited a much broader paramagnetic–ferromagnetic transition than the other two samples already at 500 Oe applied field, and thus, only a small  $\Delta S_M$  was obtained. There are several reasons for such a behavior. Additional magnetic phases and structural homogeneity may broaden the transition as discussed in Ref. [33]. Furthermore, the data for all the samples demonstrated a broad paramagnetic–ferromagnetic transition at the higher applied field of 20 kOe. That is why only the data for LCMO and LSMO were included by Hamad in Ref. [18].

Therefore, at first, we apply the new model to the said data [8, 31, 32]. As Figs. 1a and 2a show, our new approach using the asymmetric sigmoid function provides a better

suiting fitting as the original Hamad model. Figures 1b, c and 2b, c present the calculated data for  $\Delta S_M$  and  $\Delta C_{P,H}$ . The corresponding RCP values and the fitting parameters are listed in Table 1. All these data may be directly compared to the hand-calculated data presented in Ref. [8].

Then, as an example for LSMO nanowire networks, the experimental  $M(T)$  curves published in Refs. [32, 34, 35] are treated. The data comprise three different compositions, i.e.,  $\text{La}_{0.8}\text{Sr}_{0.2}\text{MnO}_3$  (the average grain size of 20.0 nm, the average diameter of 223.0 nm),  $\text{La}_{0.7}\text{Sr}_{0.3}\text{MnO}_3$  (the average grain size of 19.4 nm, the average diameter of 251.0 nm) and  $\text{La}_{0.6}\text{Sr}_{0.4}\text{MnO}_3$  (the average grain size of 24.8 nm, the average diameter of 227.8 nm), which were prepared by means of electrospinning. All the LSMO grains were randomly oriented with high-angle grain boundaries between them. The  $T_C$  varies between 314 K ( $x = 0.3$ ), 310 K ( $x = 0.4$ ) and 291 K ( $x = 0.2$ ), which confirms the excellent behavior of the  $x = 0.3$  composition. However, the  $T_C$  is lower than its bulk

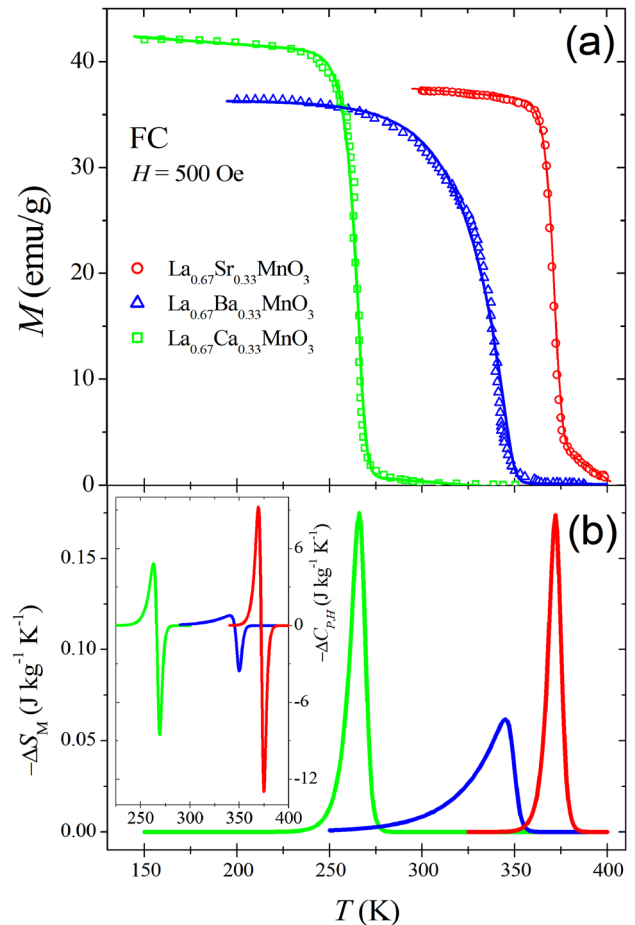


**Fig. 1** Temperature evolution of **a** the magnetization  $M$  and **b** the magnetic entropy change  $\Delta S_M$ ,  $\Delta C_{P,H}$  for LSMO, LBMO, and LCMO bulks at an applied magnetic field,  $H = 500$  Oe. The inset shows the change of the specific heat. The experimental data are from Ref. [31]. Lines are calculated using Eqs. (3), (5), and (9)

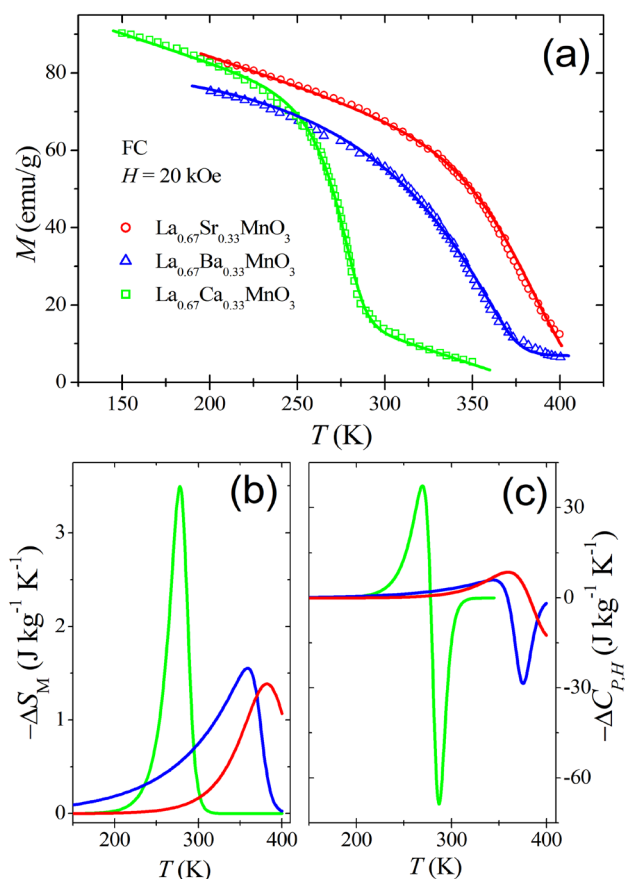


**Fig. 2** Temperature evolution of **a** the magnetization  $M$ , **b** the magnetic entropy change  $\Delta S_M$ , and **c** the change of the specific heat  $\Delta C_{P,H}$  for LSMO, LBM, and LCMO bulks at  $H = 20$  kOe. The experimental data are from Ref. [31]

counterpart as shown in Figs. 1a, b. These nanowire fabrics were characterized for their magneto-resistance behavior in Refs. [32, 34, 35]. As result, the  $M(T)$  data of all types of LSMO nanowires are well fitted by Eq. (3) as shown in Fig. 3a. The  $\Delta S_M(T)$  and  $\Delta C_{P,H}(T)$  data obtained from the experimental  $M(T)$  curves are also successfully fitted by eqs. (5) and (9), respectively, see the full lines in Fig. 3b, c.

Data of LSMO nanofibers fabricated by sol-gel electro-spinning from Ref. [36] have been previously analyzed by Hamad's model in Ref. [37]. A nonmonotonic dependence of the transition parameters has been found as the applied magnetic field  $H$  was varied between 20 Oe and 500 Oe. The authors of [36] had described their LSMO nanofibers as a collection of nanoparticles (grain size average diameter 27 nm), each with a ferrimagnetic core and a spin glass shell, organized in locally ordered clusters embedded in a disordered host. Thus, the measured  $M(T)$  curves for these nanofibers exhibit a very broad transition below  $T_C$ , in stark contrast to the bulk materials prepared by the same authors [36]. Applying our improved expressions (3–9) to these data

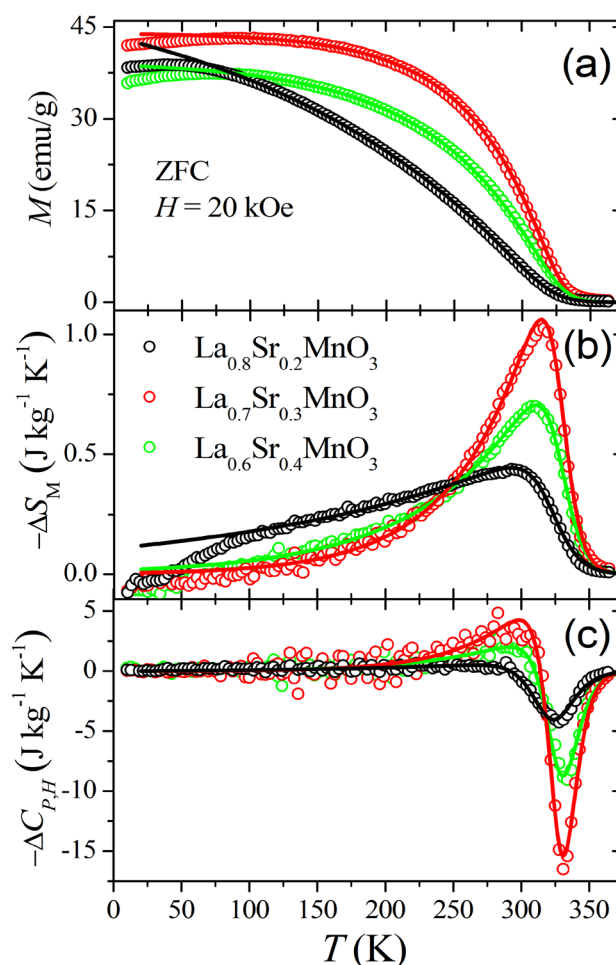


**Fig. 3** Temperature evolution of **a** the magnetization  $M$ , **b** the magnetic entropy change  $\Delta S_M$ , and **c** the change of the specific heat  $\Delta C_{P,H}$  for  $\text{La}_{1-x}\text{Sr}_x\text{MnO}_3$  nanowires with  $x$  ranging between 0.2 and 0.4; the applied magnetic field was 20 kOe. The experimental data are from Ref. [32, 34, 35]. Lines are calculated using eqs. (3), (5), and (9)

results in fitting with much better quality (see Fig. 4a). In principle, these experimental curves can be fitted with fixed  $T_w$  and shifted  $\nu$  or vice versa, or shifted both  $T_w$  and  $\nu$  for different  $H$ . Here, we use the fixed parameter  $\nu$  for different  $H$ . The predicted  $\Delta S_M(T)$  and  $\Delta C_{P,H}(T)$  dependencies are shown in Fig. 4b. The estimated parameters change monotonically with  $H$  (Table 1) instead of the results obtained in Ref. [37].

The same analysis is performed for  $M(T)$  data of  $\text{La}_{0.7}\text{Ca}_{0.3}\text{MnO}_3$  nanoparticles prepared by mechanochemical milling [38]. These nanoparticles exhibit an average diameter of 9 nm, and the dense particle agglomerates found were described by the authors as an ensemble of nanoparticles, where every individual nanoparticle possesses superspin [38], which in turn causes very broad transition curves.  $M(T)$  data for applied magnetic fields of 0.1–5 kOe were measured and 6 fields were selected for the analysis

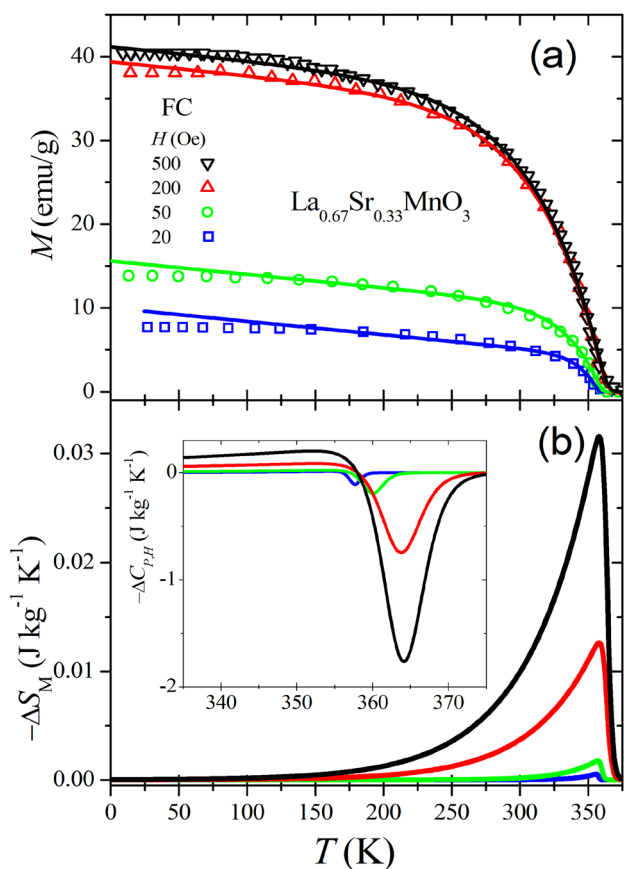


**Fig. 4** Temperature dependencies of **a** the magnetization  $M$  and **b** the magnetic entropy change  $\Delta S_M$  for LSMO nanofibers prepared in Ref. [36]. The applied magnetic fields range between 20 and 500 Oe. The inset in **(b)** shows the change of the specific heat  $\Delta C_{P,H}$

(see Table 1). The Curie temperature shifts monotonously with increasing applied field from 73 K (0.1 kOe) to 86 K (5 kOe). The fitted  $M(T)$  curves are shown in Fig. 5a. The predicted  $\Delta S_M(T)$  and  $\Delta C_{P,H}(T)$  dependencies are presented in Fig. 5b.

The  $M(T)$  data of the LSMO nanowires, nanowire fabrics and nanoparticles analyzed here are characterized by their very broad paramagnetic–ferromagnetic transitions with transition widths extending over 50–150 K, which is in stark contrast to the polycrystalline, bulk samples presented in Fig. 1a. The transition of the bulk LBMO sample of Refs. [8, 31, 32] was already an exception from this rule, thus it could serve well as an example for the application of the new formalism developed here, which was then extended to fit also the more recent data obtained for various nanomaterials using the new parameter  $\nu$ .

All the  $M(T)$  data obtained of the four different types of materials (bulks, nanowire fabrics, nanowires, nanoparticles) can be well fitted with the new formalism, see Figs. 3, 4 and 5. Thus, the application of the asymmetric Boltzmann sigmoid function represents a useful improvement to Hamad’s

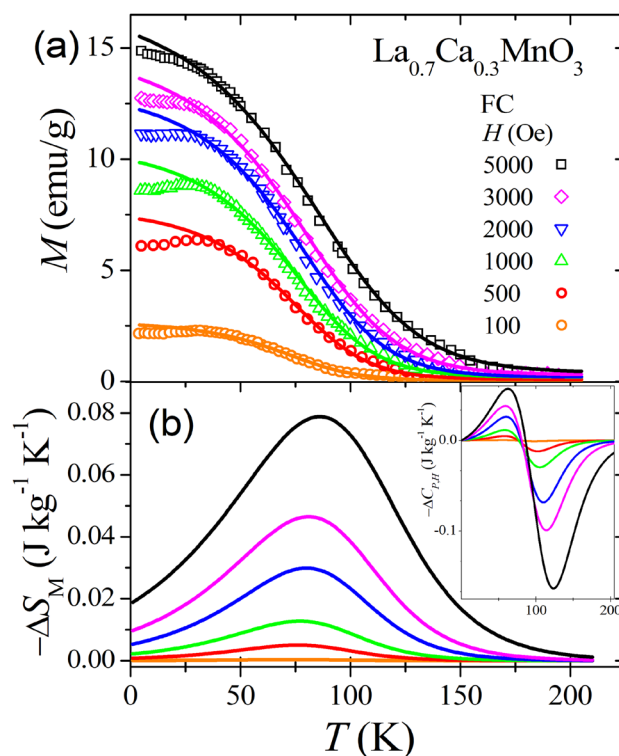


**Fig. 5** Temperature dependencies of **a** the magnetization  $M$  and **b** the magnetic entropy change  $\Delta S_M$  for LCMO nanoparticles [38]. The applied magnetic fields range between 100 and 5000 Oe. The inset to **(b)** shows the change of the specific heat  $\Delta C_{P,H}$

phenomenological model to obtain the MCE cooling parameters from magnetic  $M(T)$  measurements. The newly introduced dimensionless parameter  $\nu$ , which accounts for the asymmetry of  $M(T)$  curves, can be related to a characteristic size and structural disorder in magnetic materials. This will be a topic for future research work. We thus believe that the suggested approach can be useful also to predict the thermomagnetic parameters for any kind of transition between states with different magnetic ordering in various materials, see, e.g., the transition curves measured in Refs. [39, 40].

### 4 Conclusion

To conclude, we have introduced here a new approach to fit the experimentally obtained  $M(T)$  curves of the paramagnetic–ferromagnetic transition of MCE materials based on an asymmetric Boltzmann sigmoid function. The new model presented here provides two main advantages:

- (i) A new ansatz for the Hamad’s formula with a proper physical background. The Hamad’s formula was artificially constructed to simulate a transition curve. In contrast, our new expression makes use of the Boltz-

**Table 1** Parameters obtained from fitting of experimental  $M(T)$  data

	$\mu_0 H$ (T)	$T_C$ (K)	$T_w$ (K)	$\nu$	$M_i$ (Am <sup>2</sup> kg <sup>-1</sup> )	$\Delta S_{\text{Max}}$ (J kg <sup>-1</sup> K <sup>-1</sup> )	$\delta T_{\text{FWHM}}$ (K)	RCP (J kg <sup>-1</sup> )	$\Delta C_{P,H(\text{max})}$ (J kg <sup>-1</sup> K <sup>-1</sup> )
La <sub>0.67</sub> Sr <sub>0.33</sub> MnO <sub>3</sub> [31]	0.05	372	1.8	2	36.3	-0.17	7.8	1.3	-13
La <sub>0.67</sub> Ba <sub>0.33</sub> MnO <sub>3</sub> [31]	0.05	345	1.8	12	36	-0.062	22	1.3	-3.5
La <sub>0.67</sub> Ca <sub>0.33</sub> MnO <sub>3</sub> [31]	0.05	266	1.8	3	41	-0.175	9.2	1.6	-8.5
La <sub>0.67</sub> Sr <sub>0.33</sub> MnO <sub>3</sub> [31]	2	382	15	2	57	-1.4	65	90	-
La <sub>0.67</sub> Ba <sub>0.33</sub> MnO <sub>3</sub> [31]	2	359	6	12	82	-1.6	72	112	-29
La <sub>0.67</sub> Ca <sub>0.33</sub> MnO <sub>3</sub> [31]	2	278	5	3	71	-3.5	25	89	-69
La <sub>0.8</sub> Sr <sub>0.2</sub> MnO <sub>3</sub> [34, 35]	2	291	10	20	54.2	-0.44	183	81	-4.1
La <sub>0.7</sub> Sr <sub>0.3</sub> MnO <sub>3</sub> [34, 35]	2	314	7	8	44.0	-1.06	63	67	-15
La <sub>0.6</sub> Sr <sub>0.4</sub> MnO <sub>3</sub> [34, 35]	2	310	8	10	39.4	-0.71	84	59	-8.8
La <sub>0.67</sub> Sr <sub>0.33</sub> MnO <sub>3</sub> [36, 37]	0.002	356	0.5	27	4.4	-0.0006	12	0.007	-0.11
	0.005	357	0.9	27	10	-0.0018	21	0.037	-0.19
	0.02	358	1.7	27	34	-0.013	40	0.51	-0.75
	0.05	358	1.8	27	36	-0.032	43	1.36	-1.8
La <sub>0.7</sub> Ca <sub>0.3</sub> MnO <sub>3</sub> [38]	0.01	73	14	2	2.7	-0.0004	60	0.022	-0.001
	0.05	76	15	2	7.8	-0.0050	65	0.32	-0.012
	0.1	77	16	2	10.6	-0.013	69	0.88	-0.030
	0.2	80	17	2	13.2	-0.030	73	2.2	-0.069
	0.3	81	18.5	2	14.9	-0.047	80	3.7	-0.10
	0.5	86	21	2	17.2	-0.079	90	7.1	-0.16

mann sigmoid function, which can describe the common form of a transition between two different states.

- (ii) As a second amendment, we adapt the asymmetric Boltzmann sigmoid function for an improved description of the magnetic transition of nanosized magnetic materials by introducing a new parameter,  $\nu$ , which accounts for the asymmetry of the transition.

This approach enables a better fitting of the  $M(T)$ -data, which is especially important for the very broad transition curves of several types of nanomaterials (nanowire fabrics, nanowires, nanoparticles). A further analysis of the parameter  $\nu$  and its dependence on specific microstructures or magnetic configuration will be a task for future work. Thus, better processing of the data becomes possible to obtain reliably the MCE parameters such as  $\Delta S_M$ ,  $\Delta C_{P,H}$  and RCP from the measured  $M(T)$  curves.

**Acknowledgements** We thank X.L. Zeng (Saarland University) for providing the data of the entropy change of the LSMO nanowire networks. The model development was carried out within the State assignment of the Ministry of Science and Higher Education of the Russian Federation for the Kirensky Institute of Physics, Siberian Branch of the Russian Academy of Sciences. Part of this work was supported by the SUPERFOAM international project funded by ANR and DFG under the references ANR-17-CE05-0030 and DFG-ANR Ko2323-10,

which is gratefully acknowledged. Open Access funding enabled and organized by Projekt DEAL.

**Author Contributions** D. Gokhfeld: conceptualization, methodology, validation, formal analysis, investigation, writing–review and editing, visualization. M.R. Koblischka: conceptualization, methodology, validation, formal analysis, investigation, writing–review and editing, visualization, project administration. A. Koblischka-Veneva: methodology, formal analysis, investigation, writing–review and editing, visualization.

**Funding** Open Access funding enabled and organized by Projekt DEAL.

**Data availability** The data that support the findings of this study are available from the corresponding authors upon reasonable request.

## Declarations

**Conflict of interest** The authors declare that they have no Conflict of interest.

**Open Access** This article is licensed under a Creative Commons Attribution 4.0 International License, which permits use, sharing, adaptation, distribution and reproduction in any medium or format, as long as you give appropriate credit to the original author(s) and the source, provide a link to the Creative Commons licence, and indicate if changes were made. The images or other third party material in this article are included in the article's Creative Commons licence, unless indicated otherwise in a credit line to the material. If material is not included in the article's Creative Commons licence and your intended use is not permitted by statutory regulation or exceeds the permitted use, you will

need to obtain permission directly from the copyright holder. To view a copy of this licence, visit <http://creativecommons.org/licenses/by/4.0/>.

## References

- V.K. Pecharsky, K.A. Gschneidner Jr, Magnetocaloric Effect, in: Encyclopedia of Condensed Matter Physics, Elsevier (2005), pp. 236–244. <https://doi.org/10.1016/B0-12-369401-9/01127-X>
- K.A. Gschneidner Jr., V.K. Pecharsky, A.O. Tsokol, Recent developments in magnetocaloric materials. Rep. Prog. Phys. **68**, 1479–1539 (2005). <https://doi.org/10.1088/0034-4885/68/6/R04>
- O. Tegus, E. Brück, K.H.J. Buschow, F.R. de Boer, Transition-metal-based magnetic refrigerants for room-temperature applications. Nature **415**, 150–152 (2002). <https://doi.org/10.1038/415150a>
- T. Gottschall, K.P. Skokov, M. Fries, A. Taubel, I. Radulov, F. Scheibel, D. Benke, S. Riegg, O. Gutfleisch, Making a Cool Choice: The Materials Library of Magnetic Refrigeration. Adv. Energy Mater. **9**, 1901322 (2019). <https://doi.org/10.1002/aeam.201901322>
- J.H. Belo, A.L. Pires, J.P. Araújo, A.M. Pereira, Magnetocaloric materials: from micro- to nanoscale. J. Mater. Res. (2019). <https://doi.org/10.1557/jmr.2018.352>
- Y. Bai, X. Wu, S. Zhao, Oxygen vacancy modulating inverse and conventional magnetocaloric effects coexisting in double perovskite  $\text{Bi}_2\text{NiMnO}_{6-\delta}$  films. Ceram. Int. **47**, 6614–6622 (2021). <https://doi.org/10.1016/j.ceramint.2020.10.251>
- Y. Duan, G. Gong, M. Wang, J. Zhou, Z. Li, Y. Zuo, L. Wang, Y. Wang, Y. Su, H. Zhang, Effect of  $\text{Al}^{3+}$  substitution on the magnetodielectric properties of the one-dimensional frustrated  $\text{Ca}_3\text{Co}_2\text{O}_6$ . Phys. B **671**, 415429 (2023). <https://doi.org/10.1016/j.physb.2023.415429>
- Y. Xu, M. Meier, P. Das, M.R. Koblischka, U. Hartmann, Perovskite manganites: potential materials for magnetic cooling at or near room temperature. Cryst. Eng. **5**, 383–389 (2002). [https://doi.org/10.1016/S1463-0184\(02\)00049-7](https://doi.org/10.1016/S1463-0184(02)00049-7)
- M.H. Phan, T.L. Phan, S.C. Yu, K.W. Lee, S.H. Park, Large magnetic entropy change above 300 K in manganites. J. Korean Phys. Soc. **45**, 664–667 (2004)
- V. Anwar, S. Kumar, F. Ahmed, N. Arshi, G.W. Kim, B.H. Koo, Above room temperature magnetic transition and magnetocaloric effect in  $\text{La}_{0.66}\text{Sr}_{0.34}\text{MnO}_3$ . J. Korean Phys. Soc. **60**, 1587–1592 (2012). <https://doi.org/10.3938/jkps.60.1587>
- A.O. Ayaş, S. Kılıç Çetin, G. Akça, M. Akyol, A. Ekicibil, Magnetic refrigeration: Current progress in magnetocaloric properties of perovskite manganite materials. Mater. Today Commun. **35**, 105988 (2023). <https://doi.org/10.1016/j.mtcomm.2023.105988>
- V.E. Salazar-Muñoz, A.L. Guerrero, S.A. Palomares-Sánchez, Review of magnetocaloric properties in lanthanum manganites. J. Magn. Magn. Mat. **562**, 169787 (2022). <https://doi.org/10.1016/j.jmmm.2022.169787>
- E.L. Hernández-González, S.A. Palomares-Sánchez, J.T. Galindo, M. Mirabal-García, Magnetocaloric effect near room temperature of  $\text{La}_{0.67}\text{Ca}_{0.33-x}\text{Sr}_x\text{MnO}_3$  ( $x = 0.06, 0.07, 0.08$ ) manganites. J. Supercond. Nov. Magn. **28**, 1635–1638 (2015). <https://doi.org/10.1007/s10948-014-2932-2>
- S. Biswas, S. Keshri, Large magnetocaloric effect near room temperature in  $\text{La}_{0.67}(\text{Sr}, \text{K/Pb})_{0.33}\text{MnO}_3$  manganite nanomaterials. J. Mater. Sci. Mater. Electron. **31**, 21896–21912 (2020). <https://doi.org/10.1007/s10854-020-04694-9>
- M. Földeaki, R. Chahine, T.K. Bose, Magnetic measurements: a powerful tool in magnetic refrigerator design. J. Appl. Phys. **77**, 3528–3537 (1995). <https://doi.org/10.1063/1.358648>
- L.D. Griffith, X. Mudryk, J. Slaughter, V.K. Pecharsky, Material-based figure of merit for caloric materials. J. Appl. Phys. **123**, 034902 (2018). <https://doi.org/10.1063/1.5004173>
- M.A. Hamad, Theoretical work on magnetocaloric effect in  $\text{La}_{0.75}\text{Ca}_{0.25}\text{MnO}_3$ . J. Adv. Ceram. **1**, 290–295 (2012). <https://doi.org/10.1007/s40145-012-0027-8>
- M.A. Hamad, Prediction of thermomagnetic properties of  $\text{La}_{0.67}\text{Ca}_{0.33}\text{MnO}_3$  and  $\text{La}_{0.67}\text{Sr}_{0.33}\text{MnO}_3$ . Phase Transit. **85**, 106–112 (2012). <https://doi.org/10.1080/01411594.2011.605027>
- M.A. Hamad, Theoretical work on effect of pressure on magnetocaloric properties of  $\text{La}_{0.7}\text{Ca}_{0.3}\text{MnO}_3$ . Int. J. Thermophys. **36**, 2748–2754 (2015). <https://doi.org/10.1007/s10765-015-1960-x>
- L.H. Omari, A. Lekdadri, E.K. Hlil, H. Lassri, R. Moubah, A. Tozri, E. Dhahri, M. Kerouad, A. Zaim, Nano-sized magnetocaloric compounds investigation by using magnetization measurement and Monte Carlo simulation: Case of LSMO nanoparticles. Mater. Today Commun. **23**, 100857 (2020). <https://doi.org/10.1016/j.mtcomm.2019.100857>
- M.R. Dudek, K.K. Dudek, W. Wolak, J.N. Grima, Magnetocaloric materials with ultra-small magnetic nanoparticles working at room temperature. Sci. Rep. **9**, 17607 (2019). <https://doi.org/10.1038/s41598-019-53617-0>
- N.T.M. Duc, H.X. Shen, E.M. Clements, O. Thiabogh, J.L. Llamazares, C.F. Sanchez-Valdez, N.T. Huong, J.F. Sun, H. Srikanth, M.H. Phan, Enhanced refrigerant capacity and Curie temperature of amorphous  $\text{Gd}_{60}\text{Fe}_{20}\text{Al}_{20}$  microwires. J. Alloys. Compd. **807**, 151694 (2019). <https://doi.org/10.1016/j.jallcom.2019.151694>
- S.K. Giri, J.L. MacManus-Driscoll, W. Li, R. Wu, T.K. Nath, T.S. Maity, Strain induced extrinsic magnetocaloric effects in  $\text{La}_{0.67}\text{Sr}_{0.33}\text{MnO}_3$  thin films, controlled by magnetic field. J. Phys. D Appl. Phys. **52**, 165302 (2019). <https://doi.org/10.1088/1361-6463/ab03be>
- V. Zablotskii, Thermal partial vortex depinning and channel formation in type-II superconductors. Supercond. Sci. Technol. **14**, L25–L30 (2001). <https://doi.org/10.1088/0953-2048/14/7/102>
- T.V. Sukhareva, V.A. Finkel, Phase transition in the vortex structure of granular  $\text{YBa}_2\text{Cu}_3\text{O}_{7-\delta}$  HTSCs in weak magnetic fields. J. Exp. Theor. Phys. **107**, 787–793 (2008). <https://doi.org/10.1134/S1063776108110083>
- A.L. Navarro-Verdugo, F.M. Goycoolea, G. Romero-Meléndez, I. Higuera-Ciapara, W. Argüelles-Monal, A modified Boltzmann sigmoidal model for the phase transition of smart gels. Soft Matter **7**, 5847 (2011). <https://doi.org/10.1039/c1sm05252g>
- V.V. Derevyanko, T.V. Sukhareva, V.A. Finkel, Phase transitions and vortex structure evolution in two-level high-temperature granular superconductor  $\text{YBa}_2\text{Cu}_3\text{O}_{7-\delta}$  under temperature and magnetic field. Phys. Solid State **59**, 1492–1500 (2017). <https://doi.org/10.1134/S1063783417080091>
- D. Gokhfeld, Use of a sigmoid function to describe second peak in magnetization loops. J. Supercond. Nov. Magn. **31**, 1785–1789 (2018). <https://doi.org/10.1007/s10948-017-4400-2>
- T. Zhou, L. Peng, Y. Liu, Y. Zhan, F. Liu, A. Zhang, An insight into the sequential order in 2D correlation spectroscopy using polymer transitions: Boltzmann Sigmoid, Gaussian Cumulative, Lorentz Cumulative, and Asymmetric Sigmoid. Findings in experiments and simulations. Vib. Spectrosc. **70**, 137–161 (2014). <https://doi.org/10.1016/J.VIBSPEC.2013.12.001>
- X. Yin, J. Goudriaan, E.A. Lantinga, J. Vos, H.J. Spiertz, A flexible sigmoid function of determinate growth. Ann. Bot. **91**, 361–371 (2003). <https://doi.org/10.1093/AOB/MCG029>
- Y. Xu, U. Memmert, U. Hartmann, Thermomagnetic properties of ferromagnetic perovskite manganites. J. Magn. Magn. Mater.

- 242–245, 698–700 (2002). [https://doi.org/10.1016/S0304-8853\(01\)00999-4](https://doi.org/10.1016/S0304-8853(01)00999-4)
32. M.R. Koblischka, A. Koblischka-Veneva, J. Schmauch, Functional LSMO foams for magneto-caloric applications. *Appl. Phys. A Mater. Sci. Process.* **130**, 468 (2024). <https://doi.org/10.1007/s00339-024-07627-z>
33. K. Fabian, V.P. Shcherbakov, S.A. McEnroe, Measuring the Curie temperature. *Geochem. Geophys. Geosyst.* **14**, 947–961 (2013). <https://doi.org/10.1029/2012GC004440>
34. X.L. Zeng, T. Karwoth, A. Koblischka-Veneva, M.R. Koblischka, J. Schmauch, U. Hartmann, T. Hauet, Magnetoresistance and structural characterization of electrospun  $\text{La}_{1-x}\text{Sr}_x\text{MnO}_3$  nanowire networks. in: *Nanowires - Synthesis, Properties and Applications*, Chap. 6, S. Rackauskas (ed.), Intechopen. <https://doi.org/10.5772/intechopen.80451>
35. T. Karwoth, X.L. Zeng, M.R. Koblischka, U. Hartmann, C. Chang, T. Hauet, J.-M. Li, Magnetoresistance and structural characterization of electrospun  $\text{La}_{1-x}\text{Sr}_x\text{MnO}_3$  nanowire network fabrics with  $x = 0.2$ . *Solid State Commun.* **290**, 37–41 (2019). <https://doi.org/10.1016/j.ssc.2018.12.015>
36. R. Lu, S. Yang, Y. Li, K. Chen, Y. Jiang, B. Fu, Y. Zhang, C. Zhou, M. Xu, X. Zhou, High temperature spin-glass-like transition in  $\text{La}_{0.67}\text{Sr}_{0.33}\text{MnO}_3$  nanofibers near the Curie point. *Phys. Chem. Chem. Phys.* **19**, 16731–16736 (2017). <https://doi.org/10.1039/C7CP01276D>
37. A.H. El-Sayed, O.M. Hemed, M.A. Hamad, A.M. Mohamed, Thermomagnetic properties of  $\text{La}_{0.67}\text{Sr}_{0.33}\text{MnO}_3$  nanofibers. *Eur. Phys. J. Plus* **134**, 227 (2019). <https://doi.org/10.1140/EPJP/I2019-12751-6>
38. V. Spasojevic, A. Mrakovic, M. Perovic, V. Kusigerski, J. Blanusa, Superspin-glass like behavior of nanoparticle  $\text{La}_{0.7}\text{Ca}_{0.3}\text{MnO}_3$  obtained by mechanochemical milling. *J. Nanoparticle Res.* **13**, 763–771 (2011). <https://doi.org/10.1007/s11051-010-0076-2>
39. I.I. Makoeda, A.A. Amirov, N.A. Liedienov, A.V. Pashchenko, K.I. Yanushkevich, D.V. Yakimchuk, EYu. Kaniukov, Evolution of structure and magnetic properties in  $\text{Eu}_x\text{Bi}_{1-x}\text{FeO}_3$  multiferroics obtained under high pressure. *J. Magn. Magn. Mater.* **489**, 165379 (2019). <https://doi.org/10.1016/j.jmmm.2019.165379>
40. K. Maruyama, S. Tanaka, R. Kiyonagi, A. Nakao, K. Moriyama, Y. Ishikawa, S. Utsumi, Helimagnetism of  $\text{Ba}(\text{Fe}_{1-x}\text{Sc}_x)_{12}\text{O}_{19}$  studied by magnetization measurement and neutron diffraction. *JPS Conf. Proc.* **33**, 011061 (2021). <https://doi.org/10.7566/JPSCP.33.011061>

**Publisher's Note** Springer Nature remains neutral with regard to jurisdictional claims in published maps and institutional affiliations.